NANOPHOTONICS

Purcell effect for active tuning of light scattering from semiconductor optical antennas

Aaron L. Holsteen,[1] Søren Raza,[1] Pengyu Fan,[1] Pieter G. Kik,[1,2] Mark L. Brongersma[1]*

Subwavelength, high–refractive index semiconductor nanostructures support optical resonances that endow them with valuable antenna functions. Control over the intrinsic properties, including their complex refractive index, size, and geometry, has been used to manipulate fundamental light absorption, scattering, and emission processes in nanostructured optoelectronic devices. In this study, we harness the electric and magnetic resonances of such antennas to achieve a very strong dependence of the optical properties on the external environment. Specifically, we illustrate how the resonant scattering wavelength of single silicon nanowires is tunable across the entire visible spectrum by simply moving the height of the nanowires above a metallic mirror. We apply this concept by using a nanoelectromechanical platform to demonstrate active tuning.

High-index semiconductor nanostructures display a diverse set of optical resonances that can give rise to structural color (*1*) and facilitate effective light manipulation at the nanoscale (*2*). The optical resonances are tunable by manipulation of properties such as refractive index, size, and geometry, akin to the adaptability of metallic nanoparticles that support plasmonic resonances. A multipole analysis of the light scattering process provides valuable insights into the resonances that give rise to specific optical functionalities (*3*–*7*). We demonstrate that bringing these nanostructures into close proximity of a reflective surface can markedly enhance or suppress the interaction with selected multipoles. This is reminiscent of the Purcell effect in quantum optics, which dictates that the internal decay of an excited quantum emitter can be modified by placing it near a mirror or into a resonant cavity (*8*, *9*). From studies on quantum objects placed in tailored environments, it is also known that surface selection rules can emerge that have a substantial effect on processes such as fluorescent decay or Raman scattering (*10*). We illustrate these concepts for the lowest-order resonances of judiciously sized Si nanowires (NWs) and demonstrate active tuning of the structural color of a Si NW across the visible spectrum with a nanoelectromechanical device.

We first analyzed the white-light scattering from Si NWs above an aluminum (Al) mirror at different heights (Fig. 1A). Si NWs grown by chemical vapor deposition were deposited on a quartz substrate and then suspended above an Al-coated plano-convex lens with a large radius of curvature (r_m = 10 mm). This configuration affords nanometer-scale control over the NW height above the metal surface by sliding the quartz substrate in a plane normal to the optical axis of the Al mirror. A topographic map of this mirror was created by charting the Newton's rings resulting from the interference of monochromatic light between the air-quartz interface and the mirror (Fig. 1B) (*11*). The volume between the quartz slide and mirror was subsequently filled with an index-matching oil to produce an optically homogeneous medium around the NW.

In this configuration, the scattered light intensity from a NW is no longer just a function of the intrinsic NW properties. It is also dependent on the NW height above the mirror, as it can modify the excitation of relevant NW modes and the subsequent collection of the scattered fields by a detector. This can be seen by considering an excitation plane wave with an intensity I_0 and a wave vector of a magnitude $2\pi/\lambda$ (λ, wavelength) that is incident on the mirror at an off-normal angle ϕ. The mirror reflection generates a standing wave above the mirror (Fig. 1C). On the basis of the spatial variations in the field magnitudes, one can expect concomitant variations in the excitation efficiency of the supported NW resonances. We initially consider an idealized scenario in which the mirror is taken as a perfect electrical conductor (PEC) and the near-field interactions between the NW and substrate are neglected. This serves as a valuable reference case, as a high-conductivity Al mirror approximates a PEC and the considered NW height h in our experiments is typically sufficiently large ($2kh \gg 1$) to ensure a minimal effect of near-field interactions [supplementary text sections S1 to S3 (*12*)]. For this case, a simple expression can be written for enhancements in local electric and magnetic fields $\eta_e^{E_i}(\phi, h)$ and $\eta_e^{H_i}(\phi, h)$ of the excitation standing wave [supplementary text sections S2 and S3 (*12*)]. For off-normal incidence angles, field enhancements can be seen in both the horizontal ($\parallel$) plane and the direction normal ($\perp$) to the mirror surface, as denoted by the label i.

Similar height-dependent variations appear in the process of collecting scattered light from the NW by a finite-sized detector. These variations result from the interference between light that is directly scattered toward the detector and light entering this detector after reflecting from the surface. The strength of this interference is again dependent on h but also on the collection angle θ (*13*, *14*). These additional height-dependent variations in the measured intensity are understood from a reciprocity argument; that is, by analyzing the properties of a plane wave sent back from the location of the photodetector toward the NW and the mirror. If the resulting collection standing wave can effectively excite a NW resonance of interest, then conversely the resonantly excited NW can scatter light effectively toward the detector. The collection efficiency can be linked to the field enhancements $\eta_c^{E_i}(\theta, h)$ and $\eta_c^{H_i}(\theta, h)$ for the collection standing wave. As the scattered intensity relies on an efficient excitation followed by an efficient collection, it will be functionally dependent on products of field enhancements for the excitation and collection plane waves in the form $\eta_t^{H_i} = \eta_e^{H_i}(\phi, h)\eta_c^{H_i}(\theta, h)$ and $\eta_t^{E_i} = \eta_e^{E_i}(\phi, h)\eta_c^{E_i}(\theta, h)$. Because the excitation and collection efficiencies have different spatial periodicities, the total efficiency contains a beating pattern that depends on ϕ and θ.

For the experimentally relevant case that a detector collects light normal to the surface ($\theta = \pi$), the far-field scattered intensity (I^{ff}) can be written in an intuitive form [supplementary text sections S2 and S3 (*12*)]

$$\frac{I^{ff}(r,\phi)}{I_0} = \frac{2}{\pi k r}\begin{cases} \left|\eta_t^{H_\parallel} a_0 - 2\eta_t^{E_\parallel}\sum_{m=1,3,\ldots}\cos(m\phi)a_m + 2\eta_t^{H_\parallel}\sum_{m=2,4,\ldots}\cos(m\phi)a_m\right|^2 & \text{TE} \\ \left|\eta_t^{E_\parallel} b_0 - 2\eta_t^{H_\parallel}\sum_{m=1,3,\ldots}\cos(m\phi)b_m + 2\eta_t^{E_\parallel}\sum_{m=2,4,\ldots}\cos(m\phi)b_m\right|^2 & \text{TM} \end{cases} \quad (1)$$

where m is an integer that labels the relevant Mie coefficients a_m and b_m that quantify the excitation strength of the various multipolar resonances of a cylindrical NW illuminated in free space (*3*) and r is the observation distance. Different resonances are excited for the transverse-magnetic (TM) and transverse-electric (TE) polarizations that feature incident electric and magnetic fields parallel to the Si NW axis, respectively. When light is collected in a direction normal to the metal surface, only enhancements in the electric and magnetic fields in the horizontal plane are relevant, as they can drive NW resonances capable of scattering light upward to the detector. As such, the quantities $\eta_t^{H_\parallel}$ and $\eta_t^{E_\parallel}$ describe the relevant beating pattern of the excitation and collection plane waves that govern the scattered intensity in this experimental geometry. Depending on the symmetry properties of the relevant multipoles, the resonances are

[1]Geballe Laboratory for Advanced Materials, Stanford University, Stanford, CA 94305, USA. [2]CREOL, The College of Optics and Photonics, University of Central Florida, Orlando, FL 32816, USA.
*Corresponding author. Email: brongersma@stanford.edu

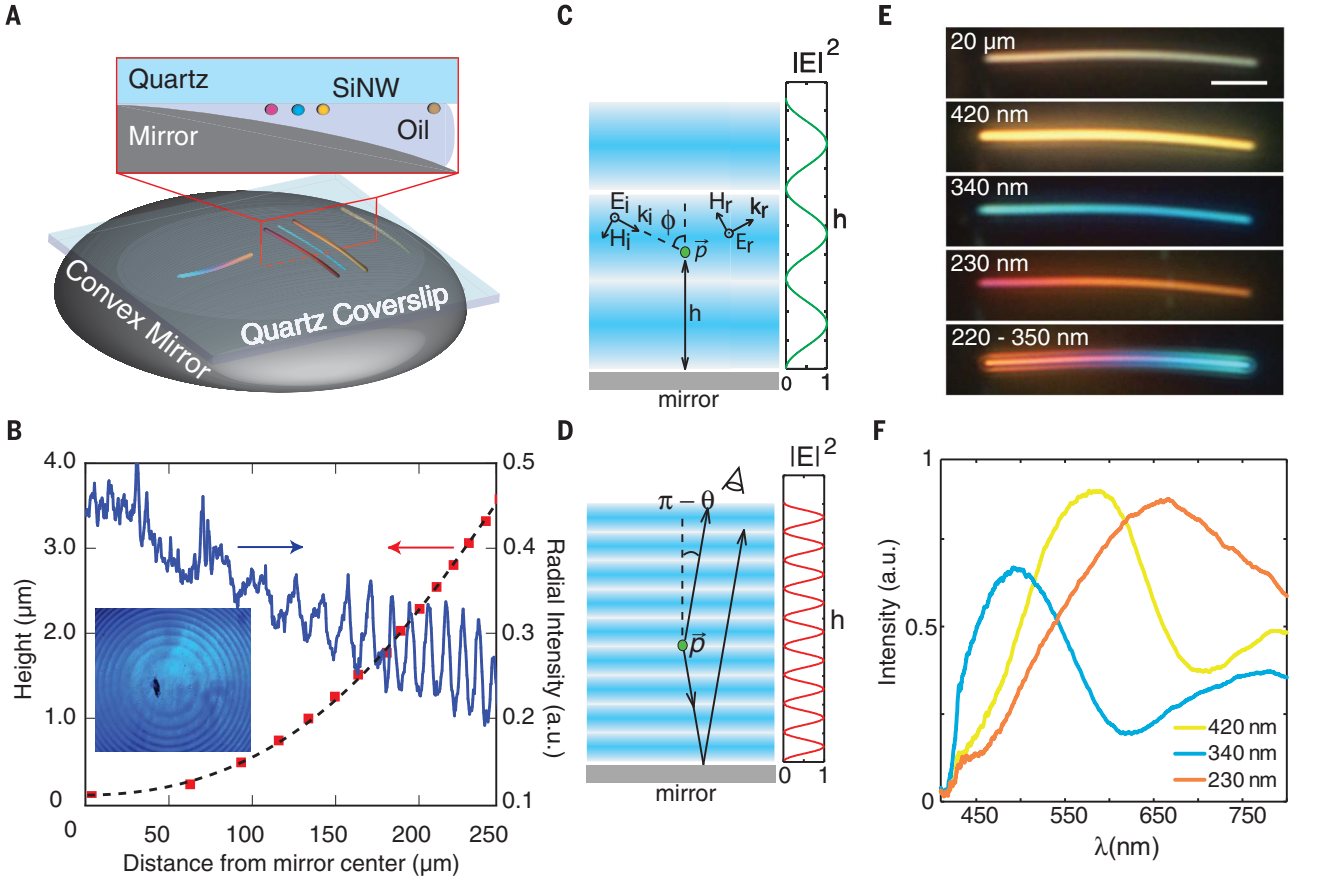

Fig. 1. Light scattering from Si NWs near a mirror. (**A**) Configuration of the suspended NWs. (**B**) Light intensity of Newton's rings (inset) imaged at 500 nm (blue trace), showing that the minimums in the interference pattern (red squares) map the parabolic mirror surface (black dashed line). a.u., arbitrary units. (**C** and **D**) Standing wave intensity from an incident (C) and collected (D) TM-polarized plane wave. E, electric field; *h*, NW height; E_i, incident electric field; k_i, incident wave vector; H_i, incident magnetic field, E_r, reflected electric field; k_r, reflected wave vector; H_r, reflected magnetic field; $\vec{p}$, dipolar scatterer; ϕ, angle of the incident plane wave; θ, collection angle. (**E**) Optical images from a single silicon NW at various heights above the mirror shown in (A). Scale bar, 5 μm. (**F**) Dark-field scattering spectra from three heights shown in (E).

most effectively excited at maximums in either the electric or magnetic field.

Figure 1E shows an example of a 50-nm–diameter Si NW that is brought toward an Al mirror. Dark-field images of this NW, using unpolarized white light, show substantial color changes as its height above the mirror changes by only a few hundred nanometers. A Si NW with a diameter this small supports only the lowest-order TM resonance with one electric field maximum in the core. It serves as a linear electric dipole, with scattering intensity governed by the Mie coefficient b_0. When the NW is 20 μm from the mirror, the NW appears white, as it features a spectrally broad resonance in the scattering efficiency (Q_{sca}). However, when the NW is closer to the mirror, the peak wavelength for this resonance is modified and can be tuned across the visible spectrum (Fig. 1F).

To systematically study the selective excitation of the first two Mie resonances for both polarizations at a range of heights, we used electron beam lithography and reactive ion etching to fabricate a 105-nm-wide and 100-μm-long Si NW (Fig. 2A). For both TE and TM polarizations (Fig. 2B), we measured and calculated the scattering efficiencies of the Si NW without the mirror (Fig. 2, C and D). The scattering calculations were performed using Mie theory for a Si cylinder in free space. The corresponding optical images of the NWs are shown next to the spectrums, displaying a uniform color. The gray dotted line represents the simulated spectrum of Q_{sca}, whereas the black dotted line denotes the partial scattering efficiency obtained by integrating the differential scattering efficiency over the collection solid angle of the objective. We find that the latter matches the experimental scattering spectra substantially better than the total scattering efficiency, indicating the importance of accounting for the anisotropic scattering properties of these NWs [supplementary text section S4 (*12*)]. The peaks in the total scattering efficiency identify the spectral locations of the supported Mie resonances. The field maps for the resonances are shown as insets and facilitate a classification according to their dipolar nature. The a_1 and b_0 Mie coefficients are associated with electric dipole (ED) resonances. Similarly, the a_0 and b_1 Mie coefficients can be linked to magnetic dipole (MD) resonances.

Light scattering spectra were taken for different wire heights above the mirror in the range from 0 to 2 μm and cascaded to create maps of the spectral and height dependent scattering properties of the NWs (Fig. 2, E and F). Adjacent to these maps, one can see the dark-field white-light scattering images of the NWs. Strong scattering is observed in the spectral region corresponding to the different Mie resonances, and the color varies substantially along the NW length. This is explained by the fact the scattering intensity at each resonance wavelength is modulated as the NW height changes. To explore the validity of the proposed analytical model, we first calculated the composite standing field profiles (i.e., $\eta_t^{H_\parallel}$ and $\eta_t^{E_\parallel}$) [supplementary text section S3 (*12*)]. The maxima in the in-plane electric (black) and magnetic (white) fields for ϕ = 37° and θ = 180° are overlaid on the map and seen to intersect experimental maxima in the scattering intensity. The strong scattering from electric (magnetic) dipole

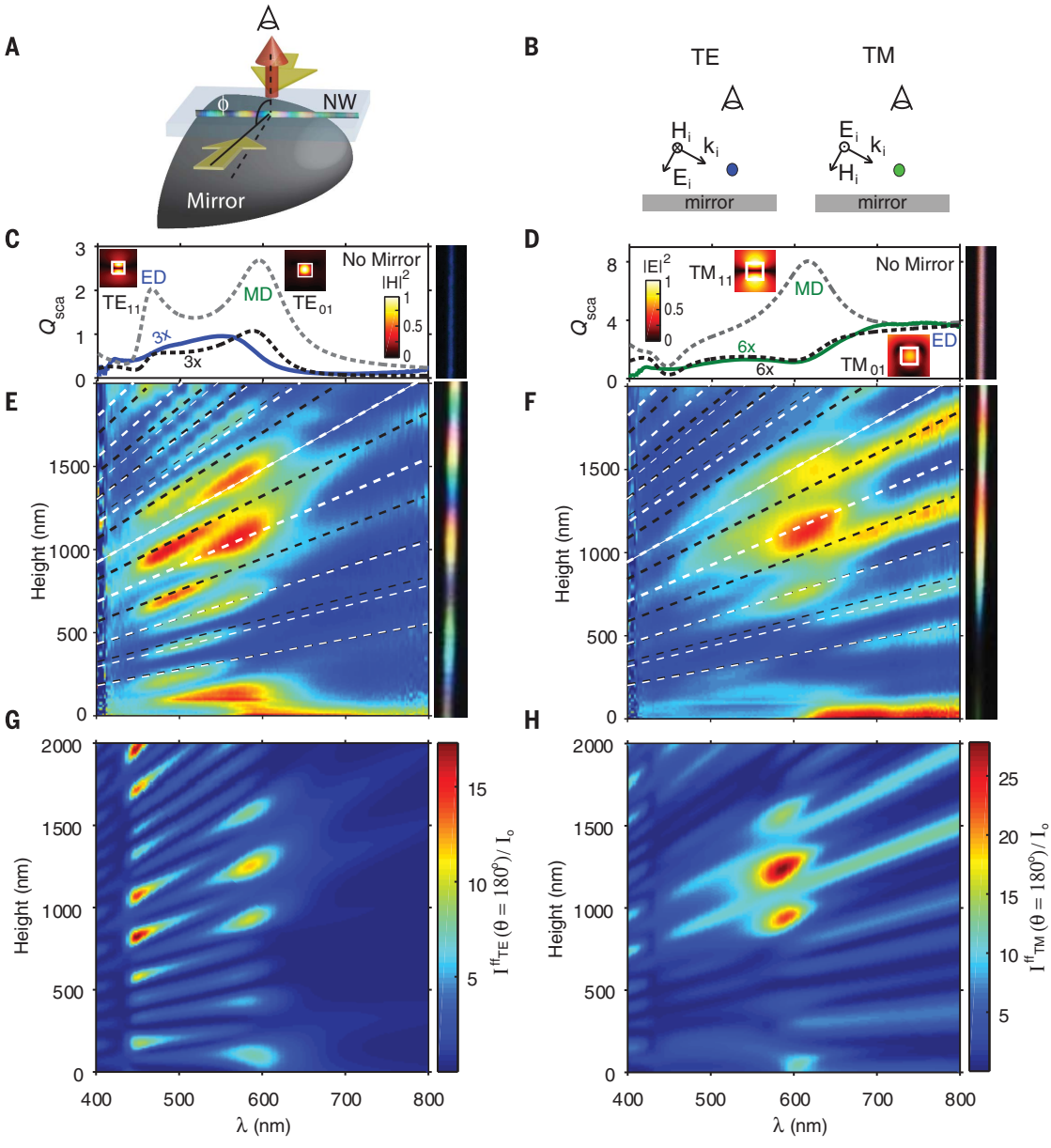

Fig. 2. Dipolar modes contributing to light scattering from a Si NW near a mirror. (**A**) Experimental configuration for the results shown in (E) to (H). ϕ is the angle of the incident plane wave. (**B**) The polarization convention for this work. (**C** and **D**) Finite-difference time-domain (FDTD) simulation of the total scattering cross section collected at all angles (gray dotted lines), with the electric and magnetic field profiles on resonance (insets) for both polarizations. The experimentally collected scattering spectrum (solid lines) and the corresponding FDTD simulated differential scattering efficiency collected within a 0.7–numerical aperture objective through the quartz handle wafer (black dotted lines). The insets show the field magnitude maps for each resonance labeled as either electric dipole–like (ED) or magnetic dipole–like (MD). Q_{sca}, scattering efficiency; TE, transverse-electric polarization; TM, transverse-magnetic polarization. (**E** and **F**) Experimentally collected light scattering spectra at heights ranging from 0 to 2000 nm for TE and TM polarization with a scale of arbitrary units. Dark-field images of the NW vertically scaled to compensate for the parabolic shape of the mirror are shown to the right of each plot. The simulated electric (black) and magnetic (white) field maxima are overlaid, with the width of the lines corresponding to the magnitude of the field maxima. (**G** and **H**) Analytic model of far-field diffracted light scattered from a Si NW above an Al mirror for both polarizations, showing the ratio of the intensity of the scattered light (I^{ff}) to the incident intensity (I_0) collected normal to the mirror plane where the observation distance is $r = 2/(\pi k)$.

resonances occurs when the NW is located at one of the electric (magnetic) field maxima. The complete solution for this experimental configuration, including real material parameters and near-field interactions, was also solved analytically using the method described in (*13*), and the far-field scattered intensities are shown in Fig. 2, G and H.

The presence of the mirror results in enhancements in light scattering that are reminiscent of the changes in Raman scattering and fluorescent emission when molecules are placed near a mirror (*8*, *9*, *15*). When the total scattered power with the mirror present is normalized by the total scattered power in free space, enhancements are observed for each mode order m

$$\mathcal{F}^{TE}_{m=0} \cong [1 + J_0(2kh)]|\eta^H_e(\phi)|^2 \quad (2)$$

$$\mathcal{F}^{TE}_{m=-1,1} \cong [1 + J_2(2kh)]|\eta^E_e(\phi)|^2 \quad (3)$$

$$\mathcal{F}^{TM}_{m=0} \cong [1 - J_0(2kh)]|\eta^E_e(\phi)|^2 \quad (4)$$

$$\mathcal{F}^{TM}_{m=-1,1} \cong [1 - J_2(2kh)]|\eta^H_e(\phi)|^2 \quad (5)$$

where J_m is the Bessel function of the first kind [supplementary text sections S6 and S7 (*12*)]. In these products, the first terms with the Bessel function describe the radiative decay rate enhancement, and the second terms ($|\eta^E_e(\phi)|^2$ or $|\eta^H_e(\phi)|^2$) quantify the excitation efficiency enhancements seen in the presence of a mirror. The decay rate enhancements are analogous to the Purcell effect and are directly connected to the local density of optical states (LDOS) [supplementary text

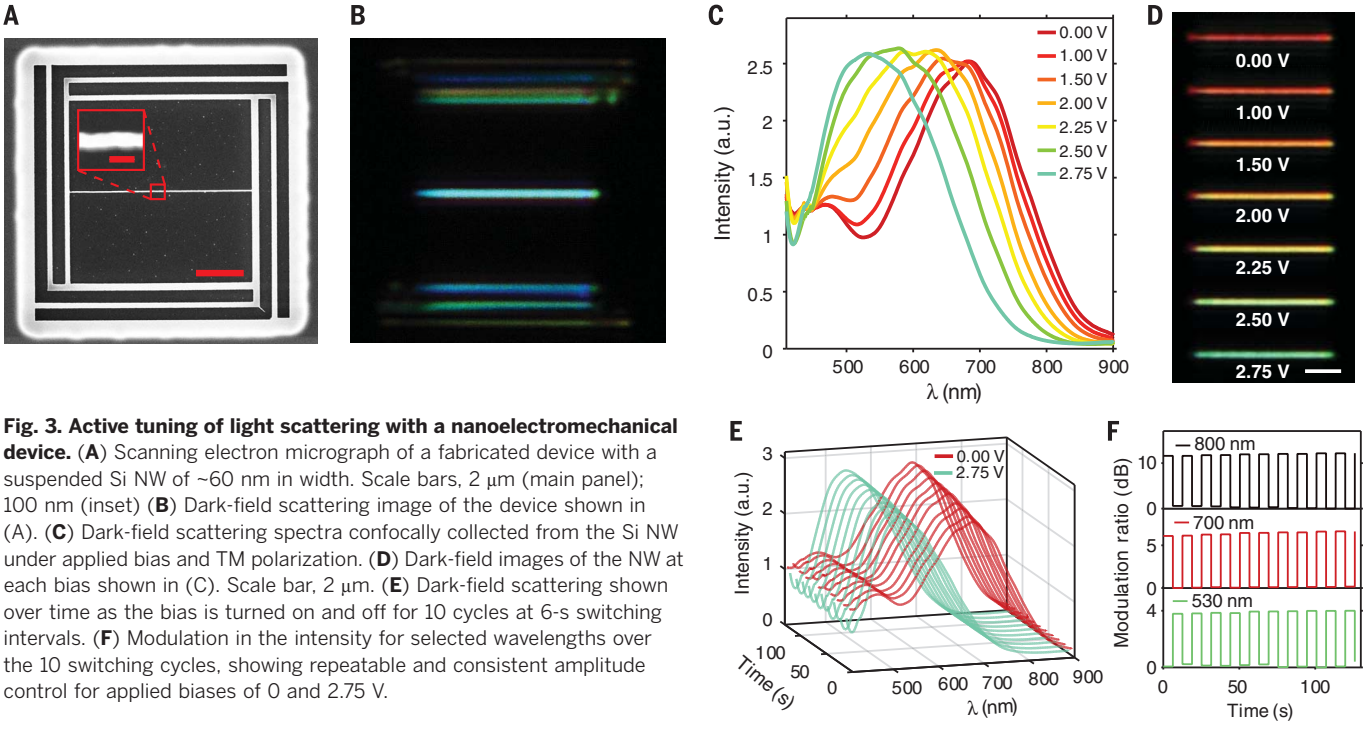

Fig. 3. Active tuning of light scattering with a nanoelectromechanical device. (**A**) Scanning electron micrograph of a fabricated device with a suspended Si NW of ~60 nm in width. Scale bars, 2 μm (main panel); 100 nm (inset) (**B**) Dark-field scattering image of the device shown in (A). (**C**) Dark-field scattering spectra confocally collected from the Si NW under applied bias and TM polarization. (**D**) Dark-field images of the NW at each bias shown in (C). Scale bar, 2 μm. (**E**) Dark-field scattering shown over time as the bias is turned on and off for 10 cycles at 6-s switching intervals. (**F**) Modulation in the intensity for selected wavelengths over the 10 switching cycles, showing repeatable and consistent amplitude control for applied biases of 0 and 2.75 V.

section S7 (*12*)]. LDOS highlights the classical nature of this effect, with the magnitude of the scattering efficiency determined by optical interference. Similarly, the Purcell effect has also been observed for Rayleigh scattering from molecules in a cavity (*16*). For selected heights, a mirror can enhance the total scattered power more than five times for $m = 0$ and more than twice for $m = \pm 1$ modes, as compared with the free-space condition for both polarizations. This enhancement in the scattering efficiency from the NW near the mirror takes into account the scattering to all directions. When only one specific far-field scattering direction is chosen, even further enhancement values can be observed. For normally incident excitation and collection from a NW, a 16-fold enhancement over the free-space scattered light intensity can be expected as the excitation and collection efficiencies are enhanced by a factor of 4.

We developed a nanoelectromechanical system (NEMS) platform to actively tune the scattering intensity and spectral properties of a NW. Reconfigurable nanomechanical structures have recently received considerable interest from the nanophotonics community for their low-power and high-frequency operation (*17*). We fabricated a 50-nm-wide Si NW with a square cross section within an underetched frame patterned into a silicon-on-insulator wafer (*12*). Such a small NW supports only the lowest-order TM resonance. The dark-field scattering shows a uniform color along its length, indicating that the NW width and height are constant (Fig. 3B). For voltages from 0 to 2.75 V, we were able to tune the single scattering peak across a large part of the visible spectrum from 700 to 520 nm (Fig. 3, C and D), in agreement with simulations (fig. S10). As long as nonreversible pull-in is avoided, the device can be reversibly tuned for more than 2 billion cycles without degradation with a maximum modulation near the fundamental mechanical resonance mode at 1 MHz (Fig. 3, E and F). For single-wavelength operation, this device can act as an intensity modulator. If we choose a spectral location such as 800 nm on the shoulder of one of the resonances, an intensity modulation ratio as large as 10 dB is achieved.

We have demonstrated how the presence of a mirror can substantially modify the excitation and collection of scattered light from NWs, even for wavelength-scale separations. These modifications are very different for the electrical and magnetic dipole resonances supported by the NWs. As a result, both the light scattering intensity and the spectral properties of suspended NWs are altered substantially. We made a rigorous link to the enhancements and suppressions associated with the Purcell effect observed for quantum objects. Looking forward, we envision that these NW devices will be used as building blocks for a range of active, integrated optoelectronic functionalities.

REFERENCES AND NOTES

1. S. Kinoshita, S. Yoshioka, *ChemPhysChem* **6**, 1442–1459 (2005).
2. A. I. Kuznetsov, A. E. Miroshnichenko, M. L. Brongersma, Y. S. Kivshar, B. Luk'yanchuk, *Science* **354**, aag2472 (2016).
3. C. Bohren, D. Huffman, *Absorption and Scattering of Light by Small Particles* (Wiley, 1983).
4. L. Novotny, B. Hecht, *Principles of Nano-Optics* (Cambridge Univ. Press, 2006).
5. L. Cao, P. Fan, M. L. Brongersma, *Nano Lett.* **11**, 1463–1468 (2011).
6. L. Cao *et al.*, *Nat. Mater.* **8**, 643–647 (2009).
7. A. B. Evlyukhin, C. Reinhardt, E. Evlyukhin, B. N. Chichkov, *J. Opt. Soc. Am. B* **30**, 2589–2598 (2013).
8. R. R. Chance, A. Prock, R. Silbey, in *Advances in Chemical Physics* (Wiley, 1978), vol. 37, pp. 1–65.
9. G. W. Ford, W. H. Weber, *Phys. Rep.* **113**, 195–287 (1984).
10. M. Moskovits, *J. Chem. Phys.* **77**, 4408–4416 (1982).
11. S. Karaveli, A. J. Weinstein, R. Zia, *Nano Lett.* **13**, 2264–2269 (2013).
12. See supplementary materials.
13. R. Borghi, M. Santarsiero, F. Frezza, G. Schettini, *J. Opt. Soc. Am. A* **14**, 1500–1504 (1997).
14. R. Borghi, F. Frezza, G. Schettini, F. Gori, M. Santarsiero, *J. Opt. Soc. Am. A* **13**, 483–493 (1996).
15. M. Moskovits, *Rev. Mod. Phys.* **57**, 783–826 (1985).
16. M. Motsch, M. Zeppenfeld, P. W. H. Pinkse, G. Rempe, *New J. Phys.* **12**, 063022 (2010).
17. N. I. Zheludev, E. Plum, *Nat. Nanotechnol.* **11**, 16–22 (2016).

ACKNOWLEDGMENTS

This research was supported by the U.S. Air Force Office of Scientific Research (grant FA9550-14-1-0389) and the Samsung corporation. A.L.H. acknowledges a National Defense Science and Engineering Graduate Fellowship. S.R. acknowledges support by a grant (VKR023371) from VILLUM FONDEN. We thank R. Zia for valuable discussions. M.L.B. and A.L.H. are inventors on patent application 62/486742 held and submitted by Stanford University that covers NEMS actuated high-index optical antennas for light manipulation and control.

SUPPLEMENTARY MATERIALS

www.sciencemag.org/content/358/6369/1407/suppl/DC1
Materials and Methods
Supplementary Text
Figs. S1 to S11
References (*18*–*20*)

31 July 2017; accepted 15 November 2017
10.1126/science.aao5371